Check for updates

ChemPlusChem

Research Article
doi.org/10.1002/cplu.202400013

Chemistry Europe
European Chemical Societies Publishing

www.chempluschem.org

CHARMM-GUI *Membrane Builder* for Lipid Droplet Modeling and Simulation

Stephen Gee,[a] Kerney Jebrell Glover,[b] Nathan J. Wittenberg,[b] and Wonpil Im*[a, b]

Lipid droplets (LDs) are organelles that are necessary for eukaryotic and prokaryotic metabolism and energy storage. They have a unique structure consisting of a spherical phospholipid monolayer encasing neutral lipids such as triacylglycerol (TAG). LDs have garnered increased interest for their implications in disease and for drug delivery applications. Consequently, there is an increased need for tools to study their structure, composition, and dynamics in biological contexts. In this work, we utilize CHARMM-GUI *Membrane Builder* to simulate and analyze LDs with and without a plant LD protein, oleosin. The results show that *Membrane Builder* can generate biologically relevant all-atom LD systems with relatively short equilibration times using a new TAG library having optimized headgroup parameters. TAG molecules originally inserted into a lipid bilayer aggregate in the membrane center, forming a TAG-only core flanked by two monolayers. The TAG-only core thickness stably grows with increasing TAG mole fraction. A 70% TAG system has a core that is thick enough to house oleosin without its interactions with the distal leaflet or disruption of its secondary structure. We hope that *Membrane Builder* can aid in the future study of LD systems, including their structure and dynamics with and without proteins.

Introduction

Lipid droplets (LDs) are essential energy-storing organelles that house neutral lipids such as triacylglycerols (TAGs) and sterol esters. The LD core is encased by a phospholipid monolayer with embedded proteins, making LDs highly diverse and structurally complex. LDs are found in a variety of prokaryotic and eukaryotic organisms and are particularly abundant in plant seeds. Therefore, understanding the nature, biogenesis, and function of LDs is important and requires an in-depth exploration at the molecular level.

The formation of LDs in eukaryotic organisms is a complex multistep process involving a host of proteins and lipids. In short, neutral lipids, which are initially evenly dispersed within the endoplasmic reticulum (ER) membrane, reach a critical concentration at which point they begin to coalesce, pushing the leaflets apart to form a lens-like structure.[1] Next, the lens-like structure is transformed into a droplet structure by membrane proteins such as seipin and lipid droplet assembly factor 1 (LDAF1).[2] Finally, the nascent LD buds off of the cytosolic leaflet of the ER membrane.

Previous molecular dynamics (MD) simulation studies have successfully modeled various steps in the LD formation process such as leaflet separation, lens-formation, and budding.[3–5] For example, Kim et al. successfully observed seipin-aided LD budding using a coarse-grained simulation of a large spherical bilayer.[3] However, long system equilibration times, limited monolayer compositions, and lack of protein incorporation in the initial system have limited the scope of these studies. Therefore, there is still an urgent need to improve and enhance MD studies of LDs.[3,6,7]

In this work, oleosin is used as a model protein to observe LD nucleation using all-atom MD simulations. Oleosin is a protein embedded in the phospholipid monolayers of plant LDs, and is thought to be particularly important for LD stabilization.[8] It consists of an amphipathic C-terminal domain, a hydrophobic hairpin that loops into the neutral lipid core of the LD, and a hydrophilic N-terminal domain.[9,10] Presumably, oleosin's unusually long hydrophobic hairpin makes it particularly well suited for LD stabilization as most other proteins do not penetrate as deeply. Therefore, successful generation of a core thickness that can accommodate oleosin can be deemed as sufficiently thick for most simulation studies.

The primary aim of this work is to demonstrate the use of CHARMM-GUI[11] *Membrane Builder*[12,13] to model and simulate LDs by utilizing an extensive TAG library and easily customizable membrane parameters. Specifically, we have added 41 TAG molecules derived from 7 different fatty acids of various chain lengths and degrees of saturation. These TAGs can be assembled into a bilayer in any combination with the other lipids available in *Membrane Builder*. To demonstrate *Membrane Builder*'s ability to build LDs, we simulated pure POPC and ER membranes with varying concentrations of triolein. Additionally, we integrated oleosin into the POPC-triolein systems to evaluate its structure and dynamics in an LD environment. This study demonstrates that *Membrane Builder* can be used to model an LD with or without proteins.

[a] S. Gee, Prof. W. Im
Departments of Biological Sciences and Bioengineering, Lehigh University, 111 Research Dr. Bethlehem, Pennsylvania, United States, 18015
E-mail: wonpil@lehigh.edu

[b] Prof. K. J. Glover, Prof. N. J. Wittenberg, Prof. W. Im
Department of Chemistry, Lehigh University, 6 E. Packer Ave Bethlehem, Pennsylvania, United States, 18015

© 2024 The Authors. ChemPlusChem published by Wiley-VCH GmbH. This is an open access article under the terms of the Creative Commons Attribution License, which permits use, distribution and reproduction in any medium, provided the original work is properly cited.

© 2024 The Authors. ChemPlusChem published by Wiley-VCH GmbH

Computational Methods

CHARMM-GUI *Membrane Builder* Implementation for Lipid Droplets

Membrane Builder supports seven lipid tails such as palmitoyl (16:0), stearoyl (18:0), oleoyl (18:1), linoleoyl (18:2), linolenoyl (18:3), aracheoyl (20:0), and gadoleoyl (20:1) that are attached to a glycerol backbone in different combinations to create 41 TAG lipid types. Within *Membrane Builder*, users can choose one of standard headgroup parameters derived from the CHARMM36 lipid force field[14] based on diacylglycerol (DAG) parameters or optimized DAG and TAG headgroup parameters (developed by Vanni and coworkers) that are relatively more hydrophobic.[15] An initial surface area of 90 Å^2 is assigned to each TAG lipid, and one can adjust the exact number or ratio of such lipids and their area if necessary.

Simulation Systems and Details

As shown in Table 1, we built and simulated a total of 10 lipid-only LD systems: 5 with POPC (palmitoyl-oleoyl phosphatidylcholine) and 5 with a lipid composition that mimics the ER membrane in Table 2.[16] All membranes are symmetric and neutralized with 0.15 M NaCl using a TIP3P water model[17] at 310 K. Each simulation was performed using OpenMM[18] and with inputs generated by *Membrane Builder*.[12,13,19,20] A six step equilibration process was followed per *Membrane Builder's* default protocol.[19] 250 ps of NVT (constant particle number, volume, and temperature) dynamics with a 1 fs time step was applied. Next, the NPT (constant particle number, pressure, and temperature) ensemble was used for a period of 125 ps with a 1 fs timestep and another period of 1.5 ns with a 2 fs time step. During equilibration, the force constants on the positions and configurations of lipid and water molecules were gradually reduced and became zero at the end of the equilibration. Five replicates were generated for each lipid-only system and the production was run for 1 μs with 4-fs time step using the hydrogen mass repartitioning technique.[20,21] We applied the SHAKE algorithm to bonds with hydrogen atoms.[22] Additionally, a force-switching function between 10 Å and 12 Å with a cutoff at 12 Å was applied to van der Waals interactions.[23] Meanwhile, electrostatic interactions were calculated using the particle-mesh Ewald method.[24] A semi-isotropic Monte Carlo barostat and Langevin dynamics friction coefficient of 1 ps^{-1} were used to maintain pressure (1 bar) and temperature (310 K).[25,26] An Alphafold[27,28] model of oleosin[29] was simulated for 1.5 μs in a mixture of 30% POPC and 70% TAG using the same simulation protocol used for the lipid-only simulations.

Table 1. Number of TAGs per leaflet of each system size.

%TAG	# Non-TAG Lipids[a]	# TAG
30%	150	64
40%	150	100
50%	150	150
60%	150	225
70%	150	350

[a] Non-TAG lipids are either POPC or ER membrane lipids in Table 2.

Table 2. ER lipid components.

Lipid Head (Tail)	Lipid Name	Number of Lipids (Outer/Inner)
PC(16:0/18:1(9Z))	POPC	24/24
PC(16:0/18:2(9Z,12Z))	PLPC	27/27
PC(18:0/20:4(5Z,8Z,11Z,14Z))	SAPC	40/40
PE(16:0/18:1(9Z))	POPE	8/8
PE(16:0/18:0)	PSPE	12/12
PE(18:0/20:4(5Z,8Z,11Z,14Z))	SAPE	10/10
PI(18:0/20:4(5Z,8Z,11Z,14Z))	SAPI	5/5
PI(18:0/18:2(9Z,12Z))	SLPI	4/4
PS(18:1(9Z)/18:2(9Z,12Z))	OLPS	5/5
SM(d18:1/16:0)	PSM	6/6
PA(16:0/18:1(9Z))	POPA	2/2
CHOL	CHOL	7/7
	TOTAL	150/150

Analysis

Each lipid-only system trajectory was analyzed for XY system dimensions, membrane thickness ($2D_c$), and deuterium order parameters (S_{cd}). Protein system trajectories were analyzed for helix tilt angles, protein-LD interaction patterns, and helicity. Each result represents the averaged value and standard error of 5 replicates for each system.

The X and Y dimensions of the system (i.e., the membrane area) were recorded as a function of time over the whole trajectory in order to assess simulation equilibration: X=Y throughout the simulation. All lipid-only systems are equilibrated before 500 ns (see Results and Discussion). $2D_c$ was measured as the difference between the average Z-positions of the first carbons on the tails of non-TAG lipids in the upper and lower leaflets. $2D_c$ was utilized as a measure of the LD core size by comparing each membrane system with a control system with no TAG. $2D_c$ was recorded as a function of time to examine the growth of the LD core over the course of the trajectory. S_{cd} quantifies the acyl chain order of lipids: $S_{cd} = <3\ \cos^2\theta\text{-}1>$, where θ is the angle between the C–H vector and the membrane normal (i.e., the Z-axis). In this study, the 16:0 *sn*-1 chain of POPC's S_{cd} was analyzed over the whole trajectory for each system.

The DSSP algorithm[30] was used to analyze the secondary structure of target oleosin residues where α-helical conformations are likely present. Analysis was run on the last 500 ns of simulation for residues predicted to be α-helices by the Alphafold model. The helix tilt angle was calculated as the angle formed between the membrane normal and the vector connecting the Cα atoms of the beginning and ending residues

© 2024 The Authors. ChemPlusChem published by Wiley-VCH GmbH

21926506, 2024, 8, Downloaded from https://chemistry-europe.onlinelibrary.wiley.com/doi/10.1002/cplu.202400013, Wiley Online Library on [31/08/2024]. See the Terms and Conditions (https://onlinelibrary.wiley.com/terms-and-conditions) on Wiley Online Library for rules of use; OA articles are governed by the applicable Creative Commons License

in each helix over the last 500 ns. Oleosin-LD interaction patterns characterize the interactions of each protein residue with certain molecules or moieties within 4 Å of the residue; they are the headgroup of phosphatidylcholine (PC) lipids, the acyl tails of PC lipids, the glycerol backbone of TAG, the acyl tails of TAG, and water. The normalized frequencies of these interactions over the last 500 ns of the trajectory are shown.

Results and Discussion

CHARMM-GUI *Membrane Builder* Provides an Easy Way to Build Lipid Droplet Models

In our previous study,[4] full TAG aggregate development took over 1-μs simulation using the standard CHARMM36 lipid force field. Furthermore, only the 60% TAG system reached an equilibrium state with a sheet-like TAG core forming at the bilayer midplane. Utilization of the optimized TAG parameters including more hydrophobic headgroup partial charges[15] in each of the lipid-only systems (Table 1, 2) resulted in a notable difference in the end states of the TAG aggregates and times required to reach them. In the current simulations, for example, equilibrium consisting of a sheet-like midplane aggregate was reached under 300 ns for all systems (Figure 1).

In both our previous and current studies, the same progression towards equilibration is observed. First, individual TAGs form small clusters that further aggregate into larger ones at the midplane after leaving the leaflets. Then, the aggregate flattens into a uniform sheet, allowing the leaflets to return to a more planar state and forming a trilayer (Figure 1A–D). Furthermore, this equilibration process is much faster, compared to about 5 μs equilibration time in the previous work that utilized pre-equilibrated bulk TAG.[31] Clearly, the LD core thickness increased correspondingly with TAG contents (Figure 1E, F) up to 60%. Unfortunately, however, all replicas of 70% lipid-only systems proved unstable and were not suitable for analysis, representing an upper limit for the TAG fraction (without protein) in our proposed protocol.

In both our previous and current studies, simulations utilizing the ER lipid composition observed a slightly faster equilibration (approximately 50 ns) than those composed of pure POPC (Figure 1G–H). This emphasizes the utility of *Membrane Builder* for generating a lipid-diverse bilayer with ease that bears a close resemblance to an actual eukaryotic LD. Additionally, modulating the target thickness of the LD core is made easy by varying the number of TAG molecules in *Membrane Builder*. We can approximate the membrane thickness contribution to the LD core by analyzing the difference between the equilibrium hydrophobic thickness (Figure 1E, F) of each system of varying TAG% with that of a pure ER membrane without TAG. Overall, the simple modularity and easy system generation using *Membrane Builder* combined with short equilibration time provide a robust and time-efficient option for LD simulation set-up.

Monolayer Properties of LDs

The lipid acyl chain order parameter, S_{cd}, was analyzed in order to assess the effects of the TAG aggregate on the order of the phospholipid tails of the bilayer. The S_{cd} values in Figure 2 indicate that POPC molecules in the TAG-ER systems are slightly more ordered, on average, than in the TAG-POPC systems. For both systems, a consistent drop in S_{cd} is evident as the percentage of TAG in the system increases, demonstrating explicit evidence of TAG's interactions with and modulation of the motion of the phospholipids in the two leaflets. Bulk TAG in the fully matured LD seems to generate interactions with each leaflet that is enough to modulate the entire phospholipid tails.

As shown in the component density analysis (Figure 3), the growth of the LD core by pushing the phospholipids outward is evident. As more TAG is introduced into the systems, its component density profile expands along the Z-axis, resulting

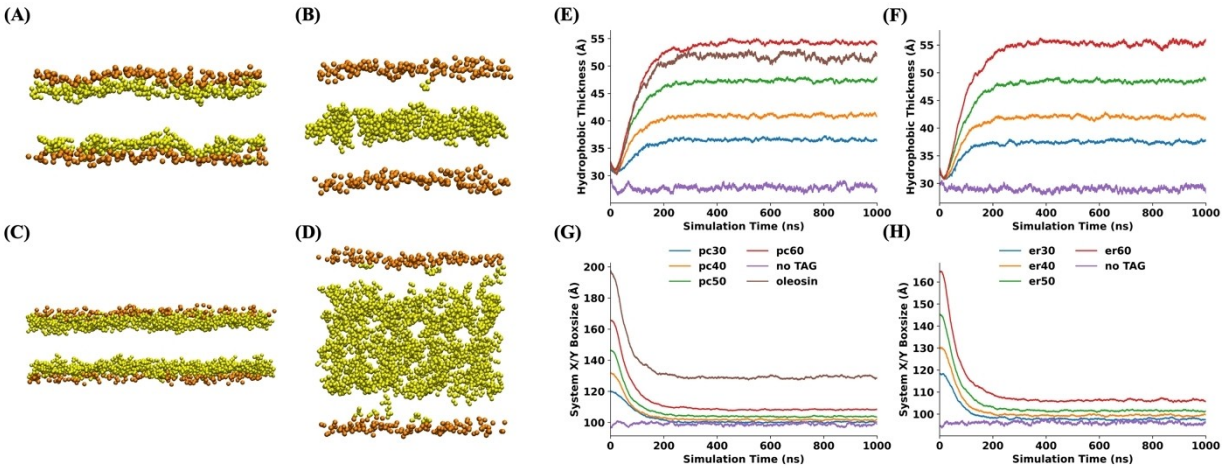

Figure 1. Snapshots of 30% TAG-POPC system at (A) 0 ns and (B) 1000 ns, and 60% TAG-ER systems at (C) 0 ns and (D) 1000 ns. In (A–D), the orange beads represent phosphorus atoms in the phospholipid heads and the yellow beads represent the glycerol oxygens in the TAG heads. Hydrophobic thickness time series of (E) TAG-POPC and (F) TAG-ER systems. X/Y system size time series of (G) TAG-POPC and (H) TAG-ER systems.

© 2024 The Authors. ChemPlusChem published by Wiley-VCH GmbH

21926506, 2024, 8, Downloaded from https://chemistry-europe.onlinelibrary.wiley.com/doi/10.1002/cplu.202400013, Wiley Online Library on [31/08/2024]. See the Terms and Conditions (https://onlinelibrary.wiley.com/terms-and-conditions) on Wiley Online Library for rules of use; OA articles are governed by the applicable Creative Commons License

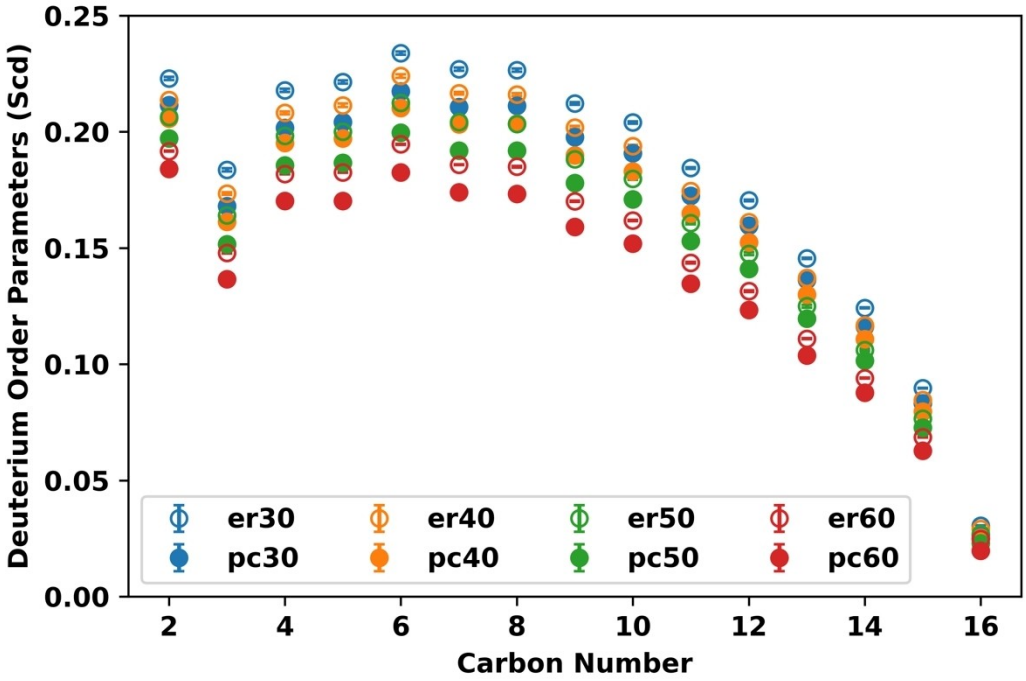

Figure 2. S_{cd} values of POPC in TAG-POPC and TAG-ER systems. Note that the errors are smaller than the symbol sizes.

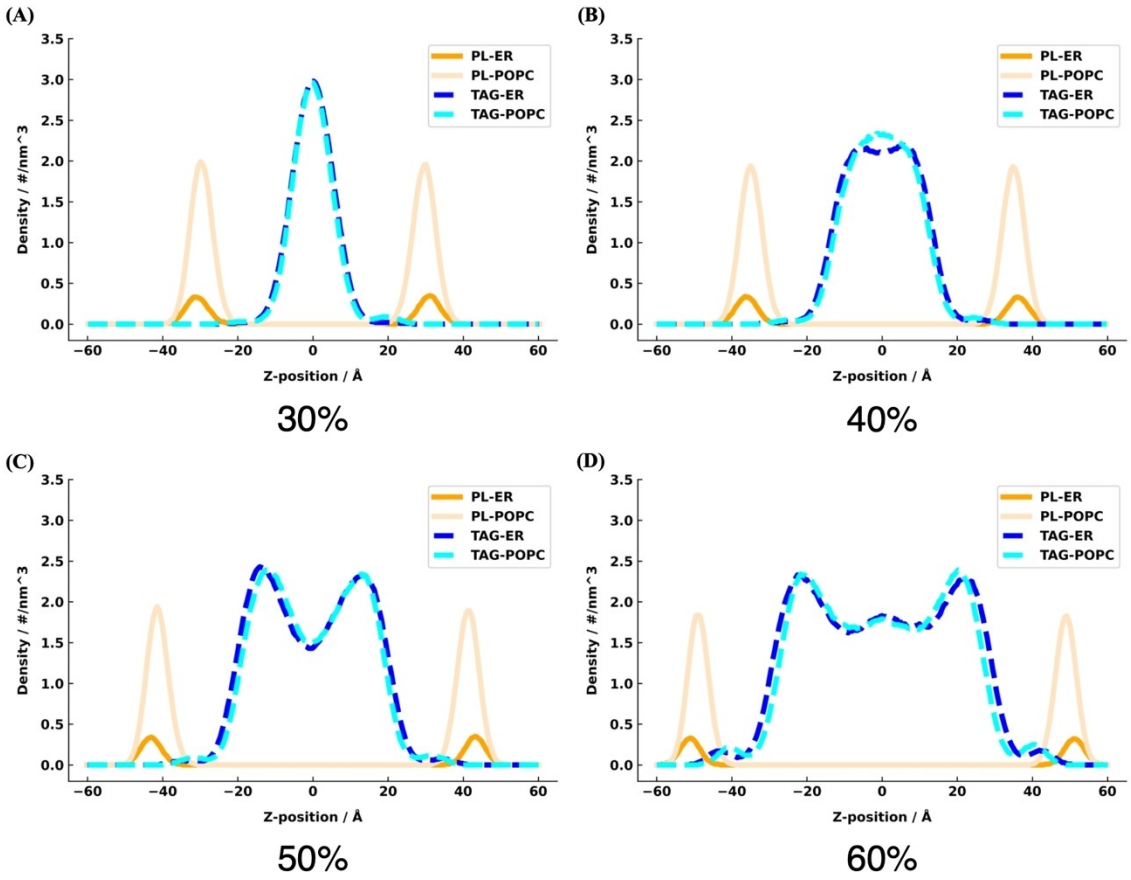

Figure 3. Component density profiles of lipid-only systems (30–60% TAG) along the Z-axis. Phospholipid densities were calculated using the phosphate atoms in the lipid head and TAG densities were calculated using the oxygens of the glycerol headgroup of TAG.

© 2024 The Authors. ChemPlusChem published by Wiley-VCH GmbH

21926506, 2024, 8, Downloaded from https://chemistry-europe.onlinelibrary.wiley.com/doi/10.1002/cplu.202400013, Wiley Online Library on [31/08/2024]. See the Terms and Conditions (https://onlinelibrary.wiley.com/terms-and-conditions) on Wiley Online Library for rules of use; OA articles are governed by the applicable Creative Commons License

in the phospholipid headgroups moving further away from the midplane. Notably, the shape of the TAG profile also transforms with higher amounts of TAG. For the 30% and 40% TAG systems, the shape follows a quasi-Gaussian distribution with the bulk of the TAG head around Z = 0 as expected. However, at 50%, there is an inversion where more TAG is centralizing closer to the interface with the ends of the phospholipid tails leaving a divot at Z = 0. This mirrors observations made in other simulations.[32,33] The 60% TAG systems show a similar shape except with a broader "valley" at Z = 0. We conclude that the TAGs located at the bimodal "peaks" are interacting with the phospholipids in each leaflet most likely via interdigitation of the TAG tails with the phospholipid tails, which would align the oxygen atoms of the TAG at a specific Z-position. Therefore, TAG located in the "valleys" (i.e., between the two "peaks") are not interacting with the phospholipid leaflets and have a more isotropic behavior.

Oleosin Properties and Behavior in LD

Our proposed strategy for simulating LDs introduces an intriguing scenario when membrane proteins come into play. Per the *Membrane Builder* protocol, the bilayer is built around any membrane proteins and hydrophilic and amphipathic regions can anchor themselves amongst polar headgroups of each leaflet. During LD simulations as the TAG aggregates between the leaflets and pushes them apart, the initial anchoring of a membrane protein in both leaflets generates an opposite "pulling" force. Because of this, it is necessary to track the stability and interactions of those proteins to ensure the validity of the equilibrium state of the LD.

In this study, simulations of oleosin were conducted in the 70% TAG-POPC membranes, as the protein-containing systems remained stable at 70% TAG, unlike their lipid-only counterparts. The TAG-POPC system is more biologically relevant to oleosin due to plant LD monolayers consisting mostly of POPC.[34] Therefore, we excluded the ER systems, although *Membrane Builder* can be used to prepare simulation systems for proteins found in mammalian LDs.

As our oleosin simulations progressed, we observed the same TAG aggregation at the bilayer midplane (Figure 4). However, there are two distinct and novel features of the oleosin simulations around and at system equilibrium. First, as the thickness of the LD core initially increased, the disordered loop (aka proline knot, PLFVIFSPIIVP) between helix 1 and helix 2 "anchored" onto the phospholipid-water interface in the trans leaflet. As a result, the protein appears to pull at the leaflet creating a cone of water molecules and phosphate groups from the POPC (Figure 4B). Importantly, the affinity of the proline knot for water and/or phosphate groups is likely not originating from the sidechains of the amino acids as they are all very hydrophobic except for one serine. Instead, it is likely through backbone interactions that are available due to the lack of secondary structure. However, upon reaching equilibrium, the protein fully separates from the trans leaflet, allowing the leaflet to relax and return to a planar formation (Figure 4C). Note that even after this relaxation, the helix proline knot is still surrounded by a few water molecules. Interestingly, we observed that these simulations reached an equilibrium TAG core thickness that was smaller than the 60% lipid-only TAG system even with a higher percentage of TAG (70%) present (Figure 1E). The amphipathic helix 3 residing within the cis leaflet significantly increases the X/Y system size (Figure 1G), which effectively decreases the membrane thickness. Perhaps, protein-lipid interactions originating from helix 3 may also explain the stability of the 70% TAG system in the presence of a protein as opposed to unstable 70% TAG simulations with no protein. Interestingly, this finding implicates a specific mechanism through which oleosin stabilizes LD droplets and future studies will validate this mechanism via experimental studies. Note that the proline knot is located within the bulk TAG region (i.e., no interactions with the trans phospholipid leaflet) at equilibrium, indicating that this LD thickness is adequate to accurately model the behavior of oleosin.

Despite oleosin's pulling interactions with the trans membrane leaflet during the equilibration process, it retains stable positioning and secondary structure at equilibrium. Helices 1 and 2 have average helicity values over 97.5% and although the amphipathic helix 3 exhibited lower average values, it remained above 90.0%. Evaluating the tilt positioning of each helix after equilibrium, each helix converges on a predominant orientation with small variations (Figure 5). This indicates a consistent and realistic hairpin conformation for oleosin in LDs.

Finally, we evaluated the interaction patterns to reinforce our observations about oleosin's equilibrium positioning rela-

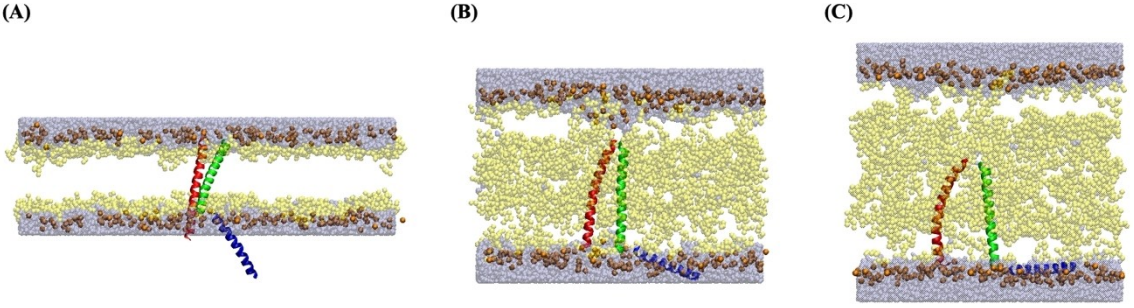

Figure 4. Progression of oleosin-TAG-POPC system at (A) 1 ns, (B) 100 ns, and (C) 1000 ns. Orange beads represent phospholipid phosphorus atoms. Yellow beads represent glycerol oxygens of TAG. Gray beads represent water. The red, green, and blue helices correspond to helix 1, 2, and 3, respectively.

© 2024 The Authors. ChemPlusChem published by Wiley-VCH GmbH

21926506, 2024, 8, Downloaded from https://chemistry-europe.onlinelibrary.wiley.com/doi/10.1002/cplu.202400013, Wiley Online Library on [31/08/2024]. See the Terms and Conditions (https://onlinelibrary.wiley.com/terms-and-conditions) on Wiley Online Library for rules of use; OA articles are governed by the applicable Creative Commons License

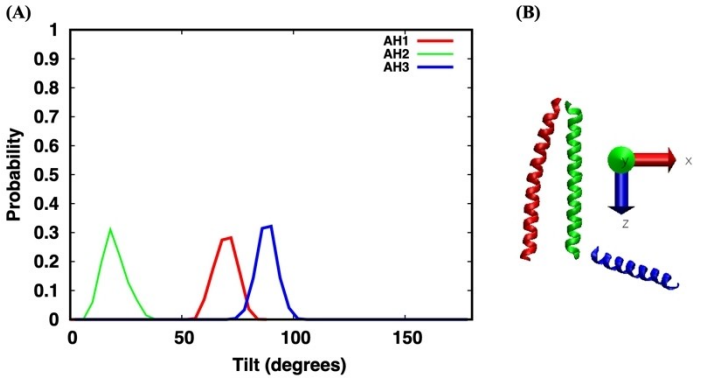

Figure 5. (A) Tilt angle distributions of oleosin α-helices in oleosin-TAG-POPC systems and (B) reference image of oleosin helices and the relative axes.

tive to the trans leaflet (Figure 6). The interaction pattern analysis supports the expected oleosin behavior at equilibrium with helices 1 and 2 in the hydrophobic hairpin primarily interacting with TAG with some interactions with phospholipid tails at residues closest to the cis leaflet. Additionally, the amphipathic helix 3 lies on the cis leaflet and interacts with PC heads, water, and PC tails along with some of the TAG heads that remain at the interface. Again, the proline knot pulls in several water molecules into the neutral lipid core from the trans leaflet. Future studies will investigate whether the associated water molecules could be biologically relevant or simply an artifact of the manner in which the protein was placed in the initial setup.

Conclusions

In this work, we have explored and examined CHARMM-GUI *Membrane Builder*'s capability for all-atom simulations of model LDs. By constructing systems of various membrane compositions and including oleosin, a LD membrane protein, we have demonstrated its ability to generate essential LD monolayer conditions in a timely manner using optimized TAG parameters. Furthermore, we described *Membrane Builder*'s ability to customize model LD simulations. All of this was accomplished within the limitations of a bilayer model of a LD. By nature of its starting bilayer state, our model comes with a tradeoff of LD core thickness for time. Increasing the maximum thickness of the equilibrated LD model by increasing the amount of starting lipids may require more time for TAG nucleation and could result in unstable systems. Additionally, this bilayer scheme is only able to model a "patch" of a fully spherical LD.

In each of our simulations, TAGs consistently aggregate at the bilayer center after approximately 250–300 ns with or without the presence of oleosin. We can modulate the thickness of this TAG monolayer by introducing varying amounts of TAG with an upper bound of 60% in lipid-only systems in our protocol. We observe that increasing amounts of TAG consistently lowers the order parameter of POPC in TAG-ER and TAG-POPC membranes. The density profile of these simulations mirrors previous studies in exhibiting the distribution pattern of TAG in the monolayer and how it transforms depending on the amount of TAG present.[31–33,35,36]

We also demonstrated that proteins can successfully be integrated into our LD simulations without the expense of secondary structures or time efficiency. Despite the harsh conditions of the growing TAG monolayer on the transmembrane protein, oleosin, it maintained its secondary structure through the simulation. With the addition of the optimized TAG parameters to *Membrane Builder*, CHARMM-GUI provides users

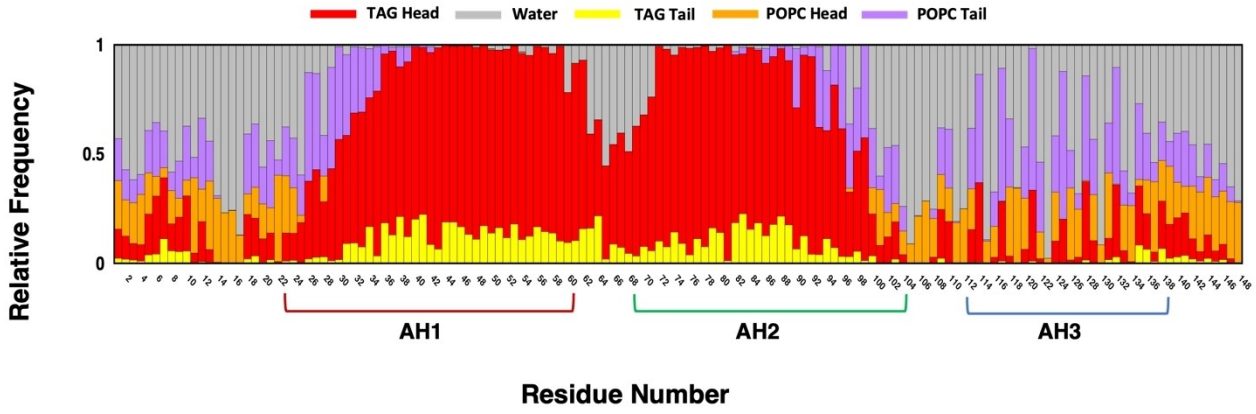

Figure 6. Interaction pattern profile of oleosin-TAG-POPC system.

© 2024 The Authors. ChemPlusChem published by Wiley-VCH GmbH

21926506, 2024, 8, Downloaded from https://chemistry-europe.onlinelibrary.wiley.com/doi/10.1002/cplu.202400013, Wiley Online Library on [31/08/2024]. See the Terms and Conditions (https://onlinelibrary.wiley.com/terms-and-conditions) on Wiley Online Library for rules of use; OA articles are governed by the applicable Creative Commons License

with the ability to generate model LD simulations with unparalleled modularity and speed. As our understanding of LD structure and function develops, we hope to continue developing this tool to make that exploration more dynamic and efficient.

Acknowledgements

The authors would like to thank Jumin Lee for implementing the TAG library on CHARMM-GUI, Hwayoung Lee for input on graphical aesthetics, and the rest of the Im lab for their continuous support. This work was partly supported by the National Science Foundation (Award #2203362) and the National Institutes of Health (GM 138472)

Conflict of Interests

W. I. is the co-founder and CEO of MolCube INC.

Data Availability Statement

The data that support the findings of this study are available from the corresponding author upon reasonable request.

Keywords: CHARMM-GUI · Lipid Droplets · Membranes · Molecular Dynamics · Oleosin

[1] J. A. Olzmann, P. Carvalho, *Nat. Rev. Mol. Cell Biol.* **2019**, *20*, 137–155.
[2] J. Chung, X. Wu, T. J. Lambert, Z. W. Lai, T. C. Walther, R. V. Farese, *Dev. Cell* **2019**, *51*, 551–563.e7.
[3] S. Kim, J. Chung, H. Arlt, A. J. Pak, R. V. Farese Jnr, T. C. Walther, G. A. Voth, *eLife* **2022**, *11*, e75808.
[4] S. Feng, L. Kong, S. Gee, W. Im, *Langmuir* **2022**, *38*, 5955–5962.
[5] H. Khandelia, L. Duelund, K. I. Pakkanen, J. H. Ipsen, *PLoS One* **2010**, *5*, e12811.
[6] V. Zoni, R. Khaddaj, I. Lukmantara, W. Shinoda, H. Yang, R. Schneiter, S. Vanni, *Proc. Natl. Acad. Sci. USA* **2021**, *118*, e2017205118.
[7] X. Prasanna, V. T. Salo, S. Li, K. Ven, H. Vihinen, E. Jokitalo, I. Vattulainen, E. Ikonen, *PLOS Biology* **2021**, *19*, e3000998.
[8] V. Parthibane, S. Rajakumari, V. Venkateshwari, R. Iyappan, R. Rajasekharan, *J. Biol. Chem.* **2012**, *287*, 1946–1954.
[9] F. Beaudoin, J. Napier, *Planta* **2002**, *215*, 293–303.
[10] D. J. Lacey, N. Wellner, F. Beaudoin, J. A. Napier, P. R. Shewry, *Biochem. J.* **1998**, *334*, 469–477.
[11] S. Jo, T. Kim, V. G. Iyer, W. Im, *J. Comput. Chem.* **2008**, *29*, 1859–1865.
[12] E. L. Wu, X. Cheng, S. Jo, H. Rui, K. C. Song, E. M. Dávila-Contreras, Y. Qi, J. Lee, V. Monje-Galvan, R. M. Venable, J. B. Klauda, W. Im, *J. Comput. Chem.* **2014**, *35*, 1997–2004.
[13] S. Jo, J. B. Lim, J. B. Klauda, W. Im, *Biophys. J.* **2009**, *97*, 50–58.
[14] J. B. Klauda, R. M. Venable, J. A. Freites, J. W. O'Connor, D. J. Tobias, C. Mondragon-Ramirez, I. Vorobyov, A. D. MacKerell Jr., R. W. Pastor, *J. Phys. Chem. B* **2010**, *114*, 7830–7843.
[15] P. Campomanes, J. Prabhu, V. Zoni, S. Vanni, *Biophys Rep (N Y)* **2021**, *1*, None.
[16] I. D. Pogozheva, G. A. Armstrong, L. Kong, T. J. Hartnagel, C. A. Carpino, S. E. Gee, D. M. Picarello, A. S. Rubin, J. Lee, S. Park, A. L. Lomize, W. Im, *J. Chem. Inf. Model.* **2022**, *62*, 1036–1051.
[17] W. Jorgensen, J. Chandrasekhar, J. Madura, R. Impey, M. Klein, *J. Chem. Phys.* **1983**, *79*, 926–935.
[18] P. Eastman, J. Swails, J. D. Chodera, R. T. McGibbon, Y. Zhao, K. A. Beauchamp, L.-P. Wang, A. C. Simmonett, M. P. Harrigan, C. D. Stern, R. P. Wiewiora, B. R. Brooks, V. S. Pande, *PLoS Comput. Biol.* **2017**, *13*, e1005659.
[19] S. Jo, T. Kim, W. Im, *PLoS One* **2007**, *2*, e880.
[20] Y. Gao, J. Lee, I. P. S. Smith, H. Lee, S. Kim, Y. Qi, J. B. Klauda, G. Widmalm, S. Khalid, W. Im, *J. Chem. Inf. Model.* **2021**, *61*, 831–839.
[21] C. W. Hopkins, S. Le Grand, R. C. Walker, A. E. Roitberg, *J. Chem. Theory Comput.* **2015**, *11*, 1864–1874.
[22] J.-P. Ryckaert, G. Ciccotti, H. J. C. Berendsen, *J. Comput. Phys.* **1977**, *23*, 327–341.
[23] P. J. Steinbach, B. R. Brooks, *J. Comput. Chem.* **1994**, *15*, 667–683.
[24] U. Essmann, L. Perera, M. L. Berkowitz, T. Darden, H. Lee, L. G. Pedersen, *J. Chem. Phys.* **1995**, *103*, 8577–8593.
[25] K.-H. Chow, D. M. Ferguson, *Comput. Phys. Commun.* **1995**, *91*, 283–289.
[26] J. Åqvist, P. Wennerström, M. Nervall, S. Bjelic, B. O. Brandsdal, *Chem. Phys. Lett.* **2004**, *384*, 288–294.
[27] M. Varadi, S. Anyango, M. Deshpande, S. Nair, C. Natassia, G. Yordanova, D. Yuan, O. Stroe, G. Wood, A. Laydon, A. Žídek, T. Green, K. Tunyasuvunakool, S. Petersen, J. Jumper, E. Clancy, R. Green, A. Vora, M. Lutfi, M. Figurnov, A. Cowie, N. Hobbs, P. Kohli, G. Kleywegt, E. Birney, D. Hassabis, S. Velankar, *Nucleic Acids Res.* **2022**, *50*, D439–D444.
[28] J. Jumper, R. Evans, A. Pritzel, T. Green, M. Figurnov, O. Ronneberger, K. Tunyasuvunakool, R. Bates, A. Žídek, A. Potapenko, A. Bridgland, C. Meyer, S. A. A. Kohl, A. J. Ballard, A. Cowie, B. Romera-Paredes, S. Nikolov, R. Jain, J. Adler, T. Back, S. Petersen, D. Reiman, E. Clancy, M. Zielinski, M. Steinegger, M. Pacholska, T. Berghammer, S. Bodenstein, D. Silver, O. Vinyals, A. W. Senior, K. Kavukcuoglu, P. Kohli, D. Hassabis, *Nature* **2021**, *596*, 583–589.
[29] J. Garcia-Mas, R. Messeguer, P. Arús, P. Puigdomènech, *Plant Mol. Biol.* **1995**, *27*, 205–210.
[30] W. Kabsch, C. Sander, *Biopolymers* **1983**, *22*, 2577–2637.
[31] S. Kim, J. M. J. Swanson, *Biophys. J.* **2020**, *119*, 1958–1969.
[32] A. Bacle, R. Gautier, C. L. Jackson, P. F. J. Fuchs, S. Vanni, *Biophys. J.* **2017**, *112*, 1417–1430.
[33] G. Henneré, P. Prognon, F. Brion, I. Nicolis, *Chem. Phys. Lipids* **2009**, *157*, 86–93.
[34] A. H. C. Huang, *Annu. Rev. Plant Physiol. Plant Mol. Biol.* **1992**, *43*, 177–200.
[35] A. Koivuniemi, M. Heikelä, P. T. Kovanen, I. Vattulainen, M. T. Hyvönen, *Biophys. J.* **2009**, *96*, 4099–4108.
[36] C. Prévost, M. E. Sharp, N. Kory, Q. Lin, G. A. Voth, R. V. Farese, T. C. Walther, *Dev. Cell* **2018**, *44*, 73–86.e4.

Manuscript received: January 7, 2024
Revised manuscript received: April 2, 2024
Accepted manuscript online: April 10, 2024
Version of record online: May 13, 2024

© 2024 The Authors. ChemPlusChem published by Wiley-VCH GmbH

21926506, 2024, 8, Downloaded from https://chemistry-europe.onlinelibrary.wiley.com/doi/10.1002/cplu.202400013, Wiley Online Library on [31/08/2024]. See the Terms and Conditions (https://onlinelibrary.wiley.com/terms-and-conditions) on Wiley Online Library for rules of use; OA articles are governed by the applicable Creative Commons License